Bioactive Ag_3PO_4/Polypropylene Composites for Inactivation of SARS-CoV-2 and another important public health pathogens

Lara K. Ribeiro[1], Marcelo Assis[1,2], Lais R. Lima[3], Dyovani Coelho[1], Mariana O. Gonçalves[4], Robert S. Paiva[3], Leonardo N. Moraes[5,6], Lauana F. Almeida[5,6], Felipe Lipsky[7], Miguel A. San-Miguel[7], Lúcia H. Mascaro[1], Rejane M. T. Grotto[5,6], Cristina P. Sousa[4], Ieda L. V. Rosa[1], Sandra A. Cruz[3], Juan Andrés[2], and Elson Longo[1]*

*e-mail: marcelostassis@gmail.com

[1]CDMF, LIEC, Federal University of São Carlos - (UFSCar), São Carlos, SP, 13565-905 Brazil

[2]Department of Physical and Analytical Chemistry, University Jaume I (UJI), Castelló 12071

[3]Chemistry Department, Federal University of São Carlos (UFSCar), São Carlos, SP, 13565-905, Brazil.

[4]Biomolecules and Microbiology Laboratory (LaMiB), Biotechnology Graduation Program, Federal University of São Carlos (UFSCar), São Carlos, SP, 13565-905, Brazil.

[5]School of Agriculture; São Paulo State University (Unesp), Botucatu, SP, 18610-034, Brazil.

[6]Molecular Laboratory of Clinical Hospital of Botucatu, Medical School; São Paulo State University (Unesp), Botucatu, SP, 18618-687, Brazil

[7]Institute of Chemistry, State University of Campinas (Unicamp), Campinas, SP, 13083-970, Brazil.

KEYWORDS: Ag_3PO_4, polypropilene, biocide composites, anti-SARS-CoV-2 composite

ABSTRACT

The current unprecedented coronavirus pandemic (COVID-19) is increasingly demanding advanced materials and new technologies to protect us and inactive the SARS-CoV-2. In this research work, we report the manufacture of Ag_3PO_4/polypropylene composites using a simple method, also revealing their long-term anti-SARS-CoV-2 activity. This composite shows superior antibacterial (against *Staphylococcus aureus* and *Escherichia coli*) and antifungal activity (against *Candida albicans*), thus having potential for a variety of technological applications. The as-manufactured materials were characterized by X-ray diffraction (XRD), Raman, Fourier transform infrared spectroscopy (FTIR), atomic force microscopy (AFM), UV–Vis, rheology, scanning electron microscopy (SEM) and contact angle to confirm their structural integrity. Based on the results of first-principles calculations at the density functional level, a plausible reaction mechanism for the initial events associated with the generation of both hydroxyl radical •OH and superoxide radical anion $\bullet O_2^-$ in the most reactive (110) surface of Ag_3PO_4 was proposed. Ag_3PO_4/polypropylene composites proved to be an attractive avenue to provide human beings with a broad spectrum of biocide activity.

1. Introduction

Currently, human beings have been facing a critical problem with the pandemic caused by the emergence of the SARS-CoV-2 virus.[1–3] Microorganisms (including bacteria, fungi and viruses) pose serious threats to public health. Particularly, viruses are one of the main causes of diseases worldwide, being responsible for infecting and killing a large part of the population in a given area.[4,5] Coronaviruses, a class of viruses, are constituted of positive single-stranded RNAs and belong to the *Coronaviridae* family.[6] The establishment of viral tropism depends on the susceptibility and permissiveness of a particular host cell. These types of viruses usually infect animals and humans due to their incredible ability to adapt to their current host, causing respiratory problems and some flu-like symptoms.[6–8]

SARS-CoV-2 is transmitted by human body fluids and the virion can entry through nasopharyngeal and/or oropharyngeal tissues.[9–13] Recent results have reported that these viruses can survive for several days on different surfaces.[14–16] In view of this scenario, efforts in research, development and manufacture of materials with anti-SARS-CoV-2 activity are growing, generating potentially safe alternatives to prevent virus contamination and transmission in humans.[17]

Innovations often play an essential role in the acceleration of the discovery of new functional materials.[18] But their success and applicability largely depend on the previous experience; our research group has been developing potent biocide materials based on complex silver-based oxides, such as Ag_2CrO_4,[19,20] three polymorphs of Ag_2WO_4,[21,22] Ag_3PO_4,[23,24] α-$AgVO_3$,[25] and β-Ag_2MoO_4[26] with enhanced antifungal activity. Additionally, to provide a deeper understanding of the atomic and electronic structure and establish a correlation between the

morphology and the biocide activity we conducted first-principles calculations at the density functional theory (DFT) level to complement and rationalize the experimental findings.[27]

Silver orthophosphate, Ag_3PO_4 (AP), is an n-type semiconductor with a band gap energy value of 2.4 eV, having high quantum efficiency until 90% for O_2 evolution from H_2O splitting.[28–34] Despite its high photocatalytic activities, notable drawbacks have emerged in relation to this material, i.e., it invariably displays a poor stability when forming metallic Ag[35–39] or dissolved in water,[40] possibly leading to partial dissociation of Ag_3PO_4 into Ag^+ and PO_4^{3-}.[41] All of these drawbacks have weakened its activity, thus reducing its broad application as a biocide agent. Very recently, Li et al. [42] have discussed and summarized the progress to improve its stability and performance, as well as the barriers that should be overcome prior to practical application.

Polypropylene (PP) is a chemically and thermally stable polymer with a wide range of applications, from textile to automotive industries, and one of the most used plastics worldwide since mid-20th century.[43] PP is used as an immobilization matrix and a substrate for biocompatibility and biocide activity tests in devices of the hospital-medical field, such as masks, aprons and food trays, among other applications.[44,45] Based on that, the strategy adopted in this work was to produce a bioactive AP/PP composite to stabilize the AP, and The inactivation of bacteria (*Staphylococcus aureus* and *Escherichia coli*), fungus (*Candida albicans*) and virus (SARS-CoV-2) have been investigated. The present composites having potential for a variety of technological applications, such as the manufacture of packaging, fabrics and protective equipment, as well as for surface treatment. The underlying technology based on this composite can be considered an innovation to protect man and avoid the contamination, transmission and proliferation of SARS-CoV-2 worldwide.

2. Methods

Ag_3PO_4 synthesis: Ag_3PO_4 was synthesized by the co-precipitation method in an aqueous medium. Separate solutions of $NaH_2PO_4.H_2O$ (98%, Sigma-Aldrich) and $AgNO_3$ (99.8%, Cennabras) were prepared with molar ratios of 1:1, respectively. The 100 mL solution of 1 x 10^{-3} mol of NaH_2PO_4 was added to the 100 mL solution of 1 x 10^{-3} mol of $AgNO_3$ under constant stirring. After the addition, the suspension was kept under stirring for 20 minutes. The precipitates were washed with deionized water and centrifuged, and this process was repeated until reaching pH neutrality (≅ 7). After the washing procedure, this powder was dried at 60 ºC for 10 h. The samples were labeled as AP.

Preparation of PP/AP composite: The composites were compounded using an internal mixer (Thermo Scientific – Polylab OS model) with a counter-rotating rotor connected to the Rheomix 600 OS Lab mixing chamber. The conditions employed were a temperature of 200 ºC and a rotor speed of 50 rpm for 4 min with closed and locked chamber, which operated with 70% of its capacity. The AP was added to the polymer (PP) in proportions of 0.5, 1.0, and 3.0% wt. The processing conditions, especially those concerning the thread profile and temperatures, were outlined to ensure an adequate dispersive and distributive mixture. The samples were named according to the AP content as follows: PP/05AP, PP/1AP and PP/3AP. The experimental characterizations, biological tests, and theoretical calculations are described in the Supporting Information (**Figures S1-S3**).

3. Results and Discussion

The XRD patterns of the PP/AP composites it is possible to observe that the alpha structure of the PP was maintained, as well as the structure of the crystals of the AP, suggesting success in

the formation of the PP/AP composites (see in Supporting Information, **Figure S4**). These results corroborate with the FTIR, micro-Raman, UV-Vis and AFM analyses, showing that at long- and short-range the structure of Ag_3PO_4 is maintained within the polymeric matrix. (**Figures S5 to S8**). The interactions between the matrix and the AP particles, as well as their dispersion state, were evaluated by rheological measurements in the dynamic state and scanning electron microscopy (SEM) conducted on cryogenically fractured samples (see **Figure 1**).

<**Insert Figure 1**>

Figure 1 - (A) Complex viscosity as a function of frequency; (B) storage modulus (G') and loss modulus (G") of the samples; and cross-section SEM images of (C) PP, (D) PP/05AP, (E) PP/1AP and (F) PP/3AP.

PP presents a pseudoplastic flow behavior with viscosity decrease as a function of frequency. A gradual increase in the viscosity of the Newtonian plateau region can be observed with the increase of the filler content. The low-frequency region named terminal zone is in the $G' \propto \omega$ and $G'' \propto \omega^2$ regions. When the degree of dispersion increases, the powers 1 and 2 change to lower values.[46] **Figure 1B** presents the same inclination values, which means low dispersion between the filler and the polymer matrix since a percolation network was not observed. These results are in accordance with the SEM images (**Figures 1C-F**). The micrography in **Figure 1C** shows the cross-section of the nanocomposites, where it is possible to observe that pristine PP is a homogeneous material. As AP is added, it is possible to see the presence of spherical particles in the nanocomposites. A better dispersion is noticed for the PP/05AP sample (**Figure 1D**). As the concentration of AP increases for PP/1AP and PP/3AP samples (**Figures 1E-F**), some micron-sized agglomerates of AP are formed, corroborating the structural data.

Figure 2 displays the contact angle results regarding the pristine PP and PP/AP composites. It is observed that for the PP sample this value is 86° and significantly increases to 98, 94 and 95° for the PP/05AP, PP/1AP and PP/3AP samples, showing statistically significant differences between samples ($p<0.05$). Since PP is an apolar polymer with hydrophobic properties,[47] by increasing the AP semiconductor content there is a consequent increase in hydrophobicity. Kasraei et al.[48] observed the same behavior in Ag-based nanocomposites in polymeric matrices. The formation of a composite with a more hydrophobic surface may inhibit and/or decrease the activities of pathogenic microorganisms as a result of the lower interaction between the composite surface and the microorganism.[49,50]

<**Insert Figure 2**>

Figure 2 - Contact angle results of pristine PP, PP/05AP, PP/1AP and PP/3AP.

Once AP was successfully incorporated into the polymeric PP matrix, contact microbicidal inhibition tests were performed. For *S. aureus* (Gram +), *E. coli* (Gram -) and *C. albicans* (fungi). The time-kill tests (**Figure 3**) were carried out, following the microbicidal evolution of the obtained materials, to corroborate the halo of inhibition tests (**Figure S9**). The analyses were performed using time variations (2, 4, 8, 16, 32, 64, 128, 256, 512, 1440 (1 day), 2880 (2 days) and 4320 min (3 days)). For *S. aureus* (**Figure 3A**), it was possible to note a reduction of 99.999% in CFU at the maximum time (3 days) for PP/3AP sample. In contrast, for *E. coli* (**Figure 3B**) there was a reduction of 99.999% at 256 min (~4.5h) for all composites. This difference between the elimination capacities of these tested bacteria was due to the fact that the composition of their membranes is very different, conferring greater resistance to the Gram + (*S. aureus*). [51–58] For the elimination of *C. albicans*, that is a more complex cellular constitution, the PP/3AP composite had contact elimination of 99% at the maximum time (3 days). For all microorganisms, it is observed

that the PP/3AP sample was more effective, inactivating at least 99% of all microorganisms (bacteria and fungus) tested.

<**Insert Figure 3**>

Figure 3 - Time–kill curves for (A) *S. aureus*, (B) *E. coli,* and (C) *C. albicans* using PP, PP/05AP, PP/1AP and PP/3AP samples.

Concerning the elimination of more complex microorganisms, tests were carried out to verify the elimination of the SARS-CoV-2 virus by placing it on the surface of contact with the composite materials obtained for 5 min (see **Figure 4**). The result of viricidal efficacy is negative when the cytopathic effects are visualized and positive when there is no cytopathic effect detected. To determine the viral inhibition index, the logarithmic difference between the control group and group in contact with the composite samples (percentage of viral elimination, compared to viral control, viral solution and DMEN) was calculated. An analysis of the results renders that the PP and PP/05 AP samples (**Figures 4A-B**) do not show viral elimination, whereas the PP/1AP and PP/3AP samples (**Figures 4C-D**) reveal 90% viral elimination. The results regarding the increasing elimination as a function of the increase in the concentration of AP in the PP are consistent with the detections expected since the microbicidal action comes from the semiconductor.[59–64] In addition, the semiconductor/polymer interaction impairs the surface fixation of pathogens in the composite, according to the contact angle results.

<**Figure 4**>

Figure 4 - Microscopic images of cell cultures incubated with viral dilutions in contact with (A) PP, (B) PP/05AP, (C) PP/1AP and (D) PP/3AP samples.

It is well established that the photocatalytic and biocide activity of a given semiconductor is dependent on the efficient formation and separation of electrons (e^-) and holes (h^+) and the low

recombination ratio of the e^--h^+ pair. It has potent antimicrobial activity, which is typically associated with the contact-induced membrane stress, are associated to the presence of reactive oxygen species (ROS), thus having potential for a variety of biomedical applications.[17,65–68]

The activations of both molecular oxygen, O_2, and water, H_2O, are fundamental step in almost all photocatalytic oxidation/reduction reactions and then the generation of ROS. At this point it is important to note the possible mechanism for the biocide activity is very dependent not only of the oxidant/reduction capacity of the different ROS, but also of the nature of the radical chain reactions. Located in the valence band of the semiconductor, the h^+ reacts with H_2O to form hydroxyl radical (•OH) and a proton (H^+), while the e^-, which is excited in the conduction band, interacts with O_2 to form $•O_2^-$. Parallel reactions involving the formation of hydrogen peroxide (H_2O_2), which is developed during the disproportionation of $•O_2^-$, can also occur, further transforming it into •OH and forming the singlet oxygen ($^1O_2$). In summary, •OH, H_2O_2, $•O_2^-$, and $^1O_2$ are generated by the stepwise oxidation of H_2O, while the stepwise reduction of O_2 generates $•O_2^-$, H_2O_2 and •OH. These free radicals and reactive species are capable of killing microorganisms by the oxidation and breaking of cellular constituents and membranes of bacteria, fungi and viruses.[69–74] The ability to generate ROSs has been explored by analyzing the adsorption processes of H_2O and O_2 molecules on the Ag_3PO_4 (110) surface. This surface has been selected because several experimental[75–79] and theoretical studies[80] report that this surface is responsible for the high catalytic activity of Ag_3PO_4.

The Ag cations on the first two layers of the clean (110) surface are low 2-fold coordinated in comparison with 4-fold coordinated Ag cations in the bulk (see **Figure 5A**). This low coordination has already been reported as having a direct correspondence with increased biocide activity, consequently activating molecules that interact with an n-type semiconductor.[81–83] The

Bader analysis of the electron density distribution[84] reveals that these Ag cations are more reduced than the innermost ones. Thus, the effective charge of the Ag_3PO_4 (110) surface from the topmost layer is +0.50-0.52 |e|, whereas the Ag bulk cations are +0.41-0.44 |e|. This fact suggests that Ag superficial cations would be preferential sites for molecular adsorption, promoting electron transfer processes to account for their lack of electron density.

<**Insert Figure 5**>

Figure 5 - (A) Side views of the relaxed clean Ag_3PO_4 (110) surface. The Ag cation where H_2O and O_2 adsorb is highlighted in black color; (B) side and top views of the H_2O adsorption system. O, P and Ag atoms on the surface are represented by red, violet and grey balls, respectively. For clarity, the O and H atoms of the H_2O are indicated in blue and white colors, respectively.

Different superficial Ag cations were considered as potential sites for the H_2O molecule adsorption. The most favorable site with a calculated adsorption energy of -1.410 eV is depicted in **Figure 5B**. This adsorption process also distorts the surface with concomitant breaking bond processes between the Ag cation and the farthest O anion. The analysis of the bond critical points (BCP) demonstrates a significant weakening of the covalent bond between the O atom of H_2O and the H closer to the surface with concomitant enlargement of the bond distance from 0.97 Å to 1.10 Å. It is also shown that the H_2O molecule establishes a second bond with the surface in the form of a weak covalent bond between its H and the nearest surface O atom. The emerging Ag-O interaction between the H_2O and the surface is characterized as van der Waals-type according to the Bader analysis. These results demonstrate that the n-type semiconductor surface activates the H_2O molecule, leading to the formation of the •OH and H^+ species.

Ab initio molecular dynamics (AIMD) simulations at low temperatures (see Supporting Information video S1 and S2) starting from the described adsorption arrangement reveal the

spontaneous breakage of the weakened O-H bond of the adsorbed H_2O molecule, corresponding to the early events associated to the formation of •OH and H^+, which remain adsorbed on the surface. There is a O-H bond involving the nearest O atom on the second layer, whereas the •OH is linked to the Ag cation on the first layer. At a higher temperature (50 K), this process occurs more rapidly, with more intense vibrational frequencies of both newly formed H-O and Ag-O bonds (**Figure 5**).

Similarly, an O_2 molecule is adsorbed on the surface at the same site with calculated adsorption energy of -1.458 eV, as shown in **Figure 6A**. After the relaxation process, the molecule displays an increased bond length from 1.23 Å (for the free molecule) to 1.30 Å, a clear indication of bond weakening caused by the interaction with the surface (**Figure 6B**). Furthermore, the total spin calculated after adsorption corresponds to a doublet oxygen (S = 1/2), differently from the triplet (S = 1) for the free O_2 molecule. These results can be associated with the initial events resulting from the formation of the $\bullet O_2^-$ in the Ag_3PO_4 (110) surface.

<Insert Figure 6>

Figure 6 - Side (A) and top (B) views of one O_2 molecule adsorbed on the Ag_3PO_4 (110) surface. O, P and Ag atoms on the surface are represented by red, violet and grey balls, respectively. For clarity, the Ag adsorption site and the water O are colored in black and blue, respectively.

4. Conclusions

Pathogen microorganisms (bacteria, fungi and viruses) represent a severe problem in public health. Therefore, there is great interest in developing advanced material and new technologies capable of inactivating opportunistic pathogens, thus reducing the risk of infection and transmission. In this work, an Ag_3PO_4/polypropylene composite was developed and optimized for

the first time. This composite has the physicochemical property of oxidizing bacteria (*Staphylococcus aureus* and *Escherichia coli*), fungi (*Candida albicans*) and SARS-COV-2 virus by surface contact. The adsorption processes of H_2O and O_2 molecules on the most active Ag_3PO_4 (110) surface were modeled through ab initio calculations to explain the early events of the formation of both hydroxyl radical •OH and superoxide radical anion $•O_2^-$ as reactive species in the biocide activity.

ASSOCIATED CONTENT

Supporting Information.

The following files are available free of charge.

Detailed experimental and theoretical procedures and structure analyses (DRX, micro-Raman, FTIR, DRS and AFM), and halo of inhibition tests. (PDF)

AIMD simulation of the activation of a water molecule on the Ag_3PO_4 (110) surface at 10 K during 900 fs (video, mpg)

AIMD simulation of the activation of a water molecule on the Ag_3PO_4 (110) surface at 50 K during 900 fs (video, mpg)

AUTHOR INFORMATION

Corresponding Author

*Marcelo Assis

CDMF, LIEC, Federal University of São Carlos - (UFSCar), São Carlos, SP, 13565-905 Brazil.

Department of Physical and Analytical Chemistry, University Jaume I (UJI), Castelló 12071.

Email: marcelostassis@gmail.com

*Juan Andres

Department of Physical and Analytical Chemistry, University Jaume I (UJI), Castelló 12071

Email: andres@fa.uji.es

*Elson Longo

CDMF, LIEC, Federal University of São Carlos - (UFSCar), São Carlos, SP, 13565-905 Brazil.

Email: elson.liec@gmail.com

Author Contributions

Lara K. Ribeiro and Marcelo Assis

Data curation, Formal analysis, Investigation, Methodology, Writing – original draft, Writing – review & editing, Visualization

Lais R. Lima, Dyovani Coelho, Robert S. Paiva, Felipe Lipsky, Mariana O. Gonçalves, Leonardo N. Moraes and Lauana F. Almeida

Data curation, Formal analysis, Methodology, Writing – original draft, Writing – review & editing, Visualization

Lúcia H. Mascaro, Rejane M. T. Grotto, Miguel A. San-Miguel, Cristina P. Sousa, Ieda L. V. Rosa, Sandra A. Cruz, Juan Andrés and Elson Longo

Funding acquisition, Resources, Supervision, Writing – original draft, Writing – review & editing, Visualization

ACKNOWLEDGMENTS

This work was funded in part by Fundação de Amparo à Pesquisa do Estado de São Paulo - FAPESP (2013/07296-2, 2016/13423-5, 2016/23891-6), 2017/26105-4, FAPESP/SHELL 2017/11986-5, 2017/07711-0), Financiadora de Estudos e Projetos - FINEP, Conselho Nacional de Desenvolvimento Cientifico e Tecnológico - CNPq (166281/2017-4 and 305792/2020-2), and Coordenação de Aperfeiçoamento de Pessoal de Nível Superior - CAPES (finance code 001). J.A. acknowledges Universitat Jaume I (project UJI-B2019-30), and the Ministerio de Ciencia, Innovación y Universidades (Spain) (project PGC2018094417-B-I00) for financially supporting this research. This work used computational resources of the "Centro Nacional de Processamento de Alto Desempenho em São Paulo" (CENAPAD-SP) and "Centro de Computação John David Rogers" (CCJDR-UNICAMP).

ABBREVIATIONS

AP (Silver phosphate, Ag_3PO_4), PP (Polypropilene), XRD (X ray diffraction), FTIR (Fourier transform infrared spectroscopy, AFM (atomic force microscopy), UV–Vis (ulttaviolet-visible), SEM (scanning electron microscopy), SARS (severe acute respiratory syndrome), MERS (Middle East respiratory syndrome), DFT (density functional theory), ICSD (Inorganic Crystal Structure Database), G' (storage modulus), G" (loss modulus), e^- (electron), h^+ (hole), E_g (band gap energy), CFU (colony-forming unit).

REFERENCES

(1) Han, Q.; Lin, Q.; Jin, S.; You, L. Coronavirus 2019-NCoV: A Brief Perspective from the Front Line. *J. Infect.* **2020**, *80* (4), 373–377. https://doi.org/10.1016/j.jinf.2020.02.010.

(2) Guan, W.; Ni, Z.; Hu, Y.; Liang, W.; Ou, C.; He, J.; Liu, L.; Shan, H.; Lei, C.; Hui, D. S. C.; et al. Clinical Characteristics of Coronavirus Disease 2019 in China. *N. Engl. J. Med.* **2020**, *382* (18), 1708–1720. https://doi.org/10.1056/NEJMoa2002032.

(3) Rothan, H. A.; Byrareddy, S. N. The Epidemiology and Pathogenesis of Coronavirus Disease (COVID-19) Outbreak. *J. Autoimmun.* **2020**, *109*, 102433. https://doi.org/10.1016/j.jaut.2020.102433.

(4) Chan, J. F. W.; Kok, K. H.; Zhu, Z.; Chu, H.; To, K. K. W.; Yuan, S.; Yuen, K. Y. Genomic Characterization of the 2019 Novel Human-Pathogenic Coronavirus Isolated from a Patient with Atypical Pneumonia after Visiting Wuhan. *Emerg. Microbes Infect.* **2020**, *9* (1), 221–236. https://doi.org/10.1080/22221751.2020.1719902.

(5) Okba, N. M. A.; Müller, M. A.; Li, W.; Wang, C.; GeurtsvanKessel, C. H.; Corman, V. M.; Lamers, M. M.; Sikkema, R. S.; de Bruin, E.; Chandler, F. D.; et al. Severe Acute

Respiratory Syndrome Coronavirus 2−Specific Antibody Responses in Coronavirus Disease Patients. *Emerg. Infect. Dis.* **2020**, *26* (7), 1478–1488. https://doi.org/10.3201/eid2607.200841.

(6) Su, S.; Wong, G.; Shi, W.; Liu, J.; Lai, A. C. K.; Zhou, J.; Liu, W.; Bi, Y.; Gao, G. F. Epidemiology, Genetic Recombination, and Pathogenesis of Coronaviruses. *Trends Microbiol.* **2016**, *24* (6), 490–502. https://doi.org/10.1016/j.tim.2016.03.003.

(7) Shi, J.; Wen, Z.; Zhong, G.; Yang, H.; Wang, C.; Huang, B.; Liu, R.; He, X.; Shuai, L.; Sun, Z.; et al. Susceptibility of Ferrets, Cats, Dogs, and Other Domesticated Animals to SARS-Coronavirus 2. *Science (80-.).* **2020**, *368* (6494), 1016–1020. https://doi.org/10.1126/science.abb7015.

(8) Li, G.; Fan, Y.; Lai, Y.; Han, T.; Li, Z.; Zhou, P.; Pan, P.; Wang, W.; Hu, D.; Liu, X.; et al. Coronavirus Infections and Immune Responses. *J. Med. Virol.* **2020**, *92* (4), 424–432. https://doi.org/10.1002/jmv.25685.

(9) Aw, J. The Non-Contact Handheld Cutaneous Infra-Red Thermometer for Fever Screening during the COVID-19 Global Emergency. *J. Hosp. Infect.* **2020**, *104* (4), 451. https://doi.org/10.1016/j.jhin.2020.02.010.

(10) Chen, H.; Guo, J.; Wang, C.; Luo, F.; Yu, X.; Zhang, W.; Li, J.; Zhao, D.; Xu, D.; Gong, Q.; et al. Clinical Characteristics and Intrauterine Vertical Transmission Potential of COVID-19 Infection in Nine Pregnant Women: A Retrospective Review of Medical Records. *Lancet* **2020**, *395* (10226), 809–815. https://doi.org/10.1016/S0140-6736(20)30360-3.

(11) Shereen, M. A.; Khan, S.; Kazmi, A.; Bashir, N.; Siddique, R. COVID-19 Infection: Origin, Transmission, and Characteristics of Human Coronaviruses. *J. Adv. Res.* **2020**, *24*, 91–98.

https://doi.org/10.1016/j.jare.2020.03.005.

(12) Qiu, L.; Liu, X.; Xiao, M.; Xie, J.; Cao, W.; Liu, Z.; Morse, A.; Xie, Y.; Li, T.; Zhu, L. SARS-CoV-2 Is Not Detectable in the Vaginal Fluid of Women with Severe COVID-19 Infection. *Clin. Infect. Dis.* **2020**, *71* (15), 813–817. https://doi.org/10.1093/cid/ciaa375.

(13) Seminara, G.; Carli, B.; Forni, G.; Fuzzi, S.; Mazzino, A.; Rinaldo, A. Biological Fluid Dynamics of Airborne COVID-19 Infection. *Rend. Lincei* **2020**, *31* (3), 505–537. https://doi.org/10.1007/s12210-020-00938-2.

(14) Razzini, K.; Castrica, M.; Menchetti, L.; Maggi, L.; Negroni, L.; Orfeo, N. V.; Pizzoccheri, A.; Stocco, M.; Muttini, S.; Balzaretti, C. M. SARS-CoV-2 RNA Detection in the Air and on Surfaces in the COVID-19 Ward of a Hospital in Milan, Italy. *Sci. Total Environ.* **2020**, *742*, 140540. https://doi.org/10.1016/j.scitotenv.2020.140540.

(15) Wu, S.; Wang, Y.; Jin, X.; Tian, J.; Liu, J.; Mao, Y. Environmental Contamination by SARS-CoV-2 in a Designated Hospital for Coronavirus Disease 2019. *Am. J. Infect. Control* **2020**, *48* (8), 910–914. https://doi.org/10.1016/j.ajic.2020.05.003.

(16) Vardoulakis, S.; Sheel, M.; Lal, A.; Gray, D. COVID-19 Environmental Transmission and Preventive Public Health Measures. *Aust. N. Z. J. Public Health* **2020**, *44* (5), 333–335. https://doi.org/10.1111/1753-6405.13033.

(17) Tremiliosi, G. C.; Simoes, L. G. P.; Minozzi, D. T.; Santos, R. I.; Vilela, D. C. B.; Durigon, E. L.; Machado, R. R. G.; Medina, D. S.; Ribeiro, L. K.; Rosa, I. L. V.; et al. Ag Nanoparticles-Based Antimicrobial Polycotton Fabrics to Prevent the Transmission and Spread of SARS-CoV-2. *bioRxiv* **2020**, https://doi.org/10.1101/2020.06.26.152520.

(18) Gupta, A.; Mumtaz, S.; Li, C.-H.; Hussain, I.; Rotello, V. M. Combatting Antibiotic-Resistant Bacteria Using Nanomaterials. *Chem. Soc. Rev.* **2019**, *48* (2), 415–427.

https://doi.org/10.1039/C7CS00748E.

(19) Assis, M.; de Foggi, C. C.; Teodoro, V.; Costa, J. P.C.; Silva, C. E.; Robeldo, T.; Caperucci, P. F.; Vergani, C. E.; Borra, R. C.; Sorribes, I.; et al. Surface-Dependent Photocatalytic and Biological Activities of Ag_2CrO_4: Integration of Experiment and Simulation. *Appl. Surf. Sci.* **2021**, *545*, 148964. https://doi.org/10.1016/j.apsusc.2021.148964.

(20) Pinatti, I. M.; Tello, A. C. M.; Trench, A. B.; de Foggi, C. C.; Pereira, P. F. S.; Teixeira, M. M.; Jacomaci, N.; Andrés, J.; Longo, E. Zinc-Substituted Ag_2CrO_4: A Material with Enhanced Photocatalytic and Biological Activity. *J. Alloys Compd.* **2020**, *835*, 155315. https://doi.org/https://doi.org/10.1016/j.jallcom.2020.155315.

(21) Alvarez-Roca, R.; Gouveia, A. F.; de Foggi, C. C.; Lemos, P. S.; Gracia, L.; da Silva, L. F.; Vergani, C. E.; San-Miguel, M.; Longo, E.; Andrés, J. Selective Synthesis of α-, β-, and γ-Ag_2WO_4 Polymorphs: Promising Platforms for Photocatalytic and Antibacterial Materials. *Inorg. Chem.* **2021**, *60* (2), 1062–1079. https://doi.org/10.1021/acs.inorgchem.0c03186.

(22) Foggi, C. C.; Fabbro, M. T.; Santos, L. P. S.; de Santana, Y. V. B.; Vergani, C. E.; Machado, A. L.; Cordoncillo, E.; Andrés, J.; Longo, E. Synthesis and Evaluation of α-Ag_2WO_4 as Novel Antifungal Agent. *Chem. Phys. Lett.* **2017**, *674*, 125–129. https://doi.org/10.1016/j.cplett.2017.02.067.

(23) Filho, J. F. C.; Lima, T. M. S.; Lima, M. S.; Nolêto, L. F. G.; Bandeira, C. S.; Lima, F. L.; Luz, G. E. Microorganisms Photocatalytic Inactivation on Ag_3PO_4 Sub-Microcrystals Under WLEDs Light Source. *J. Inorg. Organomet. Polym. Mater.* **2021**, *31*, 2233. https://doi.org/10.1007/s10904-021-01930-5.

(24) de Foggi, C. C.; de Oliveira, R. C.; Fabbro, M. T.; Vergani, C. E.; Andres, J.; Longo, E.; Machado, A. L. Tuning the Morphological, Optical, and Antimicrobial Properties of α-

Ag_2WO_4 Microcrystals Using Different Solvents. *Cryst. Growth Des.* **2017**, *17* (12), 6239–6246. https://doi.org/10.1021/acs.cgd.7b00786.

(25) de Oliveira, R. C.; de Foggi, C. C.; Teixeira, M. M.; da Silva, M. D. P.; Assis, M.; Francisco, E. M.; Pimentel, B. N. A. da S.; Pereira, P. F. dos S.; Vergani, C. E.; Machado, A. L.; et al. Mechanism of Antibacterial Activity via Morphology Change of α-$AgVO_3$: Theoretical and Experimental Insights. *ACS Appl. Mater. Interfaces* **2017**, *9* (13), 11472–11481. https://doi.org/10.1021/acsami.7b00920.

(26) De Foggi, C. C.; De Oliveira, R. C.; Assis, M.; Fabbro, M. T.; Mastelaro, V. R.; Vergani, C. E.; Gracia, L.; Andrés, J.; Longo, E.; Machado, A. L. Unvealing the Role of β-Ag_2MoO_4 Microcrystals to the Improvement of Antibacterial Activity. *Mater. Sci. Eng. C* **2020**, *111* (September 2018), 110765. https://doi.org/10.1016/j.msec.2020.110765.

(27) Gouveia, A. F.; Gracia, L.; Longo, E.; San-Miguel, M. A.; Andrés, J. Modulating the Properties of Multifunctional Semiconductors by Means of Morphology: Theory Meets Experiments. *Comput. Mater. Sci.* **2021**, *188*, 110217. https://doi.org/10.1016/j.commatsci.2020.110217.

(28) Yi, Z.; Ye, J.; Kikugawa, N.; Kako, T.; Ouyang, S.; Stuart-Williams, H.; Yang, H.; Cao, J.; Luo, W.; Li, Z.; et al. An Orthophosphate Semiconductor with Photooxidation Properties under Visible-Light Irradiation. *Nat. Mater.* **2010**, *9* (7), 559–564. https://doi.org/10.1038/nmat2780.

(29) Zhang, H.; Huang, H.; Ming, H.; Li, H.; Zhang, L.; Liu, Y.; Kang, Z. Carbon Quantum Dots/Ag_3PO_4 Complex Photocatalysts with Enhanced Photocatalytic Activity and Stability under Visible Light. *J. Mater. Chem.* **2012**, *22* (21), 10501–10506. https://doi.org/10.1039/c2jm30703k.

(30) Botelho, G.; Andres, J.; Gracia, L.; Matos, L. S.; Longo, E. Photoluminescence and Photocatalytic Properties of Ag_3PO_4 Microcrystals: An Experimental and Theoretical Investigation. *Chempluschem* **2016**, *81* (2), 202–212. https://doi.org/10.1002/cplu.201500485.

(31) Trench, A. B.; Machado, T. R.; Gouveia, A. F.; Foggi, C. C.; Teodoro, V.; Sánchez-Montes, I.; Teixeira, M. M.; Da Trindade, L. G.; Jacomaci, N.; Perrin, A.; et al. Rational Design of W-Doped Ag_3PO_4 as an Efficient Antibacterial Agent and Photocatalyst for Organic Pollutant Degradation. *ACS Omega* **2020**, *5* (37), 23808–23821. https://doi.org/10.1021/acsomega.0c03019.

(32) Rakibuddin, M.; Ananthakrishnan, R. A Novel Ag Deposited Nanocoordination Polymer Derived Porous SnO_2/NiO Heteronanostructure for the Enhanced Photocatalytic Reduction of Cr(VI) under Visible Light. *New J. Chem.* **2016**, *40* (4), 3385–3394. https://doi.org/10.1039/c5nj02755a.

(33) Dinh, C. T.; Nguyen, T. D.; Kleitz, F.; Do, T. O. Large-Scale Synthesis of Uniform Silver Orthophosphate Colloidal Nanocrystals Exhibiting High Visible Light Photocatalytic Activity. *Chem. Commun.* **2011**, *47* (27), 7797–7799. https://doi.org/10.1039/c1cc12014j.

(34) Huang, K.; Lv, Y.; Zhang, W.; Sun, S.; Yang, B.; Chi, F.; Ran, S.; Liu, X. One-Step Synthesis of Ag_3PO_4/Ag Photocatalyst with Visible-Light Photocatalytic Activity. *Mater. Res.* **2015**, *18* (5), 939–945. https://doi.org/10.1590/1516-1439.346614.

(35) Costa, T. M. S.; Lima, M. S.; Cruz Filho, J. F.; Silva, L. J.; Santos, R. S.; Luz, G. E. Synthesis, Characterization, and Photocatalytic Activity of Ag_3PO_4/SBA-15 in Ciprofloxacin Degradation under Polychromatic Irradiation. *J. Photochem. Photobiol. A Chem.* **2018**, *364* (February), 461–471. https://doi.org/10.1016/j.jphotochem.2018.06.039.

(36) Cruz-Filho, J. F.; Costa, T. M. S.; Lima, M. S.; Silva, L. J.; Santos, R. S.; Cavalcante, L. S.; Longo, E.; Luz, G. E. Effect of Different Synthesis Methods on the Morphology, Optical Behavior, and Superior Photocatalytic Performances of Ag_3PO_4 Sub-Microcrystals Using White-Light-Emitting Diodes. *J. Photochem. Photobiol. A Chem.* **2019**, *377*, 14–25. https://doi.org/10.1016/j.jphotochem.2019.03.031.

(37) Costa, J. P. C.; Assis, M.; Teodoro, V.; Rodrigues, A.; de Foggi, C.; San-Miguel, M. A.; Carmo, J. P. P.; Andrés, J.; Longo, E. Electron Beam Irradiation for the Formation of Thick Ag Film on Ag_3PO_4. *RSC Adv.* **2020**, *10* (37), 21745–21753. https://doi.org/10.1039/d0ra03179h.

(38) Santos, C. C.; Assis, M.; Machado, T. R.; Pereira, P. F. S.; Minguez-Vega, G.; Cordoncillo, E.; Beltran-Mir, H.; Doñate-Buendía, C.; Andrés, J.; Longo, E. Proof-of-Concept Studies Directed toward the Formation of Metallic Ag Nanostructures from Ag_3PO_4 Induced by Electron Beam and Femtosecond Laser. *Part. & Part. Syst. Charact.* **2019**, *36* (6), 1800533. https://doi.org/10.1002/ppsc.201800533.

(39) Botelho, G.; Sczancoski, J. C.; Andres, J.; Gracia, L.; Longo, E. Experimental and Theoretical Study on the Structure, Optical Properties, and Growth of Metallic Silver Nanostructures in Ag_3PO_4. *J. Phys. Chem. C* **2015**, *119* (11), 6293–6306. https://doi.org/10.1021/jp512111v.

(40) Guo, R.; Wu, J.; Xu, A.; Huang, X.; Zhu, H.; Jiang, R.; Lin, Y.; Guo, F. $ZnWO_4/Ag_3PO_4$ Composites with an Enhanced Photocatalytic Activity and Stability under Visible Light. *RSC Adv.* **2016**, *6* (115), 114818–114824. https://doi.org/10.1039/c6ra19180k.

(41) Hsieh, M.-S.; Su, H.-J.; Hsieh, P.-L.; Chiang, Y.-W.; Huang, M. H. Synthesis of Ag_3PO_4 Crystals with Tunable Shapes for Facet-Dependent Optical Property, Photocatalytic

Activity, and Electrical Conductivity Examinations. *ACS Appl. Mater. Interfaces* **2017**, *9* (44), 39086–39093. https://doi.org/10.1021/acsami.7b13941.

(42) Li, X.; Xu, P.; Chen, M.; Zeng, G.; Wang, D.; Chen, F.; Tang, W.; Chen, C.; Zhang, C.; Tan, X. Application of Silver Phosphate-Based Photocatalysts: Barriers and Solutions. *Chem. Eng. J.* **2019**, *366*, 339–357. https://doi.org/10.1016/j.cej.2019.02.083.

(43) Kamal, M. M.; Safan, M. A.; Etman, Z. A.; Kasem, B. M. Mechanical Properties of Self-Compacted Fiber Concrete Mixes. *HBRC J.* **2014**, *10*, 25–34. https://doi.org/10.1016/j.hbrcj.2013.05.012.

(44) Ghaffari, M.; Mollazadeh-Bajestani, M.; Moztarzadeh, F.; Uludağ, H.; Hardy, J. G.; Mozafari, M. An Overview of the Use of Biomaterials, Nanotechnology, and Stem Cells for Detection and Treatment of COVID-19: Towards a Framework to Address Future Global Pandemics. *Emergent Mater.* **2021**, *4*, 19–34. https://doi.org/10.1007/s42247-020-00143-9.

(45) Martí, M.; Tuñón-Molina, A.; Aachmann, F. L.; Muramoto, Y.; Noda, T.; Takayama, K.; Serrano-Aroca, Á. Protective Face Mask Filter Capable of Inactivating SARS-CoV-2, and Methicillin-Resistant Staphylococcus Aureus and Staphylococcus Epidermidis. *Polymers (Basel).* **2021**, *13* (2), 1–12. https://doi.org/10.3390/polym13020207.

(46) Abraham, J.; Sharika, T.; George, S. C.; Thomas, S. Rheology : Open Access Rheological Percolation in Thermoplastic Polymer Nanocomposites. *Rheol. Open access* **2017**, *1* (1), 1–15.

(47) Terpilowski, K.; Rymuszka, D.; Holysz, L.; Chibowski, E. Changes in Wettability of Polycarbonate and Polypropylene Pretreated With Oxygen and Argon Plasma. *Proc. 8th Int. Conf. MMT* **2014**, *4*, 155–165.

(48) Kasraei, S.; Azarsina, M. Addition of Silver Nanoparticles Reduces the Wettability of Methacrylate and Silorane-Based Composites. *Braz. Oral Res.* **2012**, *26* (6), 505–510. https://doi.org/10.1590/S1806-83242012000600004.

(49) Liu, Q.; Brookbank, L.; Ho, A.; Coffey, J.; Brennan, A. B.; Jones, C. J. Surface Texture Limits Transfer of S. Aureus, T4 Bacteriophage, Influenza B Virus and Human Coronavirus. *PLoS One* **2021**, *15*, 1–19. https://doi.org/10.1371/journal.pone.0244518.

(50) Hosseini, M.; Chin, A. W. H.; Behzadinasab, S.; Poon, L. L. M.; Ducker, W. A. Cupric Oxide Coating That Rapidly Reduces Infection by SARS-CoV-2 via Solids. *ACS Appl. Mater. Interfaces* **2021**, *13* (5), 5919. https://doi.org/10.1021/acsami.0c19465.

(51) Piccirillo, C.; Pinto, R. A.; Tobaldi, D. M.; Pullar, R. C.; Labrincha, J. A.; Pintado, M. M. E.; Castro, P. M. L. Light Induced Antibacterial Activity and Photocatalytic Properties of Ag_3PO4-Based Material of Marine Origin. *J. Photochem. Photobiol. A Chem.* **2015**, *296*, 40–47. https://doi.org/10.1016/j.jphotochem.2014.09.012.

(52) Gherasim, O.; Puiu, R. A.; Bîrca, A. C.; Burduşel, A. C.; Grumezescu, A. M. An Updated Review on Silver Nanoparticles in Biomedicine. *Nanomaterials* **2020**, *10* (11), 1–44. https://doi.org/10.3390/nano10112318.

(53) Liou, J. W.; Chang, H. H. Bactericidal Effects and Mechanisms of Visible Light-Responsive Titanium Dioxide Photocatalysts on Pathogenic Bacteria. *Arch. Immunol. Ther. Exp. (Warsz)*. **2012**, *60* (4), 267–275. https://doi.org/10.1007/s00005-012-0178-x.

(54) Macedo, N. G.; Machado, T. R.; Roca, R. A.; Assis, M.; Foggi, C. C.; Puerto-Belda, V.; Mínguez-Vega, G.; Rodrigues, A.; San-Miguel, M. A.; Cordoncillo, E.; et al. Tailoring the Bactericidal Activity of Ag Nanoparticles/α-Ag_2WO_4 Composite Induced by Electron Beam and Femtosecond Laser Irradiation: Integration of Experiment and Computational

Modeling. *ACS Appl. Bio Mater.* **2019**, *2*, 824–837. https://doi.org/10.1021/acsabm.8b00673.

(55) Roca, R. A.; Sczancoski, J. C.; Nogueira, I. C.; Fabbro, M. T.; Alves, H. C.; Gracia, L.; Santos, L. P. S.; De Sousa, C. P.; Andrés, J.; Luz, G. E.; et al. Facet-Dependent Photocatalytic and Antibacterial Properties of α-Ag_2WO_4 Crystals: Combining Experimental Data and Theoretical Insights. *Catal. Sci. Technol.* **2015**, *5* (8), 4091–4107. https://doi.org/10.1039/c5cy00331h.

(56) Abram, S.-L.; Fromm, K. M. Handling (Nano)Silver as Antimicrobial Agent: Therapeutic Window, Dissolution Dynamics, Detection Methods and Molecular Interactions. *Chem. A Eur. J.* **2020**, *26* (48), 10948–10971. https://doi.org/10.1002/chem.202002143.

(57) Choi, Y.; Kim, H.-A.; Kim, K.-W.; Lee, B.-T. Comparative Toxicity of Silver Nanoparticles and Silver Ions to Escherichia Coli. *J. Environ. Sci.* **2018**, *66*, 50–60. https://doi.org/10.1016/j.jes.2017.04.028.

(58) Berlanga, M.; Montero, M. T.; Hernández-Borrell, J.; Viñas, M. Influence of the Cell Wall on Ciprofloxacin Susceptibility in Selected Wild-Type Gram-Negative and Gram-Positive Bacteria. *Int. J. Antimicrob. Agents* **2004**, *23* (6), 627–630. https://doi.org/10.1016/j.ijantimicag.2003.12.015.

(59) Barzegar, H.; Zahed, M. A.; Vatanpour, V. Antibacterial and Antifouling Properties of Ag_3PO_4/GO Nanocomposite Blended Polyethersulfone Membrane Applied in Dye Separation. *J. Water Process Eng.* **2020**, *38*, 101638. https://doi.org/10.1016/j.jwpe.2020.101638.

(60) Tamiyakul, H.; Roytrakul, S.; Jaresitthikunchai, J.; Phaonakrop, N.; Tanasupawat, S.; Warisnoicharoen, W. Changes in Protein Patterns of Staphylococcus Aureus and

Escherichia Coli by Silver Nanoparticles Capped with Poly (4-Styrenesulfonic Acid-Co-Maleic Acid) Polymer. *Asian Biomed.* **2019**, *13* (2), 39–47. https://doi.org/10.1515/abm-2019-0039.

(61) Salleh, A.; Naomi, R.; Utami, N. D.; Mohammad, A. W.; Mahmoudi, E.; Mustafa, N.; Fauzi, M. B. The Potential of Silver Nanoparticles for Antiviral and Antibacterial Applications: A Mechanism of Action. *Nanomaterials* **2020**, *10* (8), 1566. https://doi.org/10.3390/nano10081566.

(62) Nakamura, S.; Sato, M.; Sato, Y.; Ando, N.; Takayama, T.; Fujita, M.; Ishihara, M. Synthesis and Application of Silver Nanoparticles (Ag NPs) for the Prevention of Infection in Healthcare Workers. *Int. J. Mol. Sci.* **2019**, *20* (15), 3620. https://doi.org/10.3390/ijms20153620.

(63) Kubo, A.-L.; Capjak, I.; Vrček, I. V.; Bondarenko, O. M.; Kurvet, I.; Vija, H.; Ivask, A.; Kasemets, K.; Kahru, A. Antimicrobial Potency of Differently Coated 10 and 50 Nm Silver Nanoparticles against Clinically Relevant Bacteria Escherichia Coli and Staphylococcus Aureus. *Colloids Surfaces B Biointerfaces* **2018**, *170*, 401–410. https://doi.org/10.1016/j.colsurfb.2018.06.027.

(64) Chang, B. M.; Pan, L.; Lin, H. H.; Chang, H. C. Nanodiamond-Supported Silver Nanoparticles as Potent and Safe Antibacterial Agents. *Sci. Rep.* **2019**, *9* (1), 1–11. https://doi.org/10.1038/s41598-019-49675-z.

(65) Basak, S.; Packirisamy, G. Nano-Based Antiviral Coatings to Combat Viral Infections. *Nano-Structures and Nano-Objects* **2020**, *24*, 100620. https://doi.org/10.1016/j.nanoso.2020.100620.

(66) Mukherjee, S.; Mazumder, P.; Joshi, M.; Joshi, C.; Dalvi, S. V.; Kumar, M. Biomedical

Application, Drug Delivery and Metabolic Pathway of Antiviral Nanotherapeutics for Combating Viral Pandemic: A Review. *Environ. Res.* **2020**, *191*, 110119. https://doi.org/10.1016/j.envres.2020.110119.

(67) Jeremiah, S. S.; Miyakawa, K.; Morita, T.; Yamaoka, Y.; Ryo, A. Potent Antiviral Effect of Silver Nanoparticles on SARS-CoV-2. *Biochem. Biophys. Res. Commun.* **2020**, *533* (1), 195–200. https://doi.org/10.1016/j.bbrc.2020.09.018.

(68) Assis, M.; Simoes, L. G. P.; Tremiliosi, G. C.; Coelho, D.; Minozzi, D. T.; Santos, R. I.; Vilela, D. C. B.; Rodrigues, J.; Ribeiro, L. K.; Rosa, I.L.V. et al. SiO_2-Ag Composite as a Highly Virucidal Material : A Roadmap That Rapidly Eliminates SARS-CoV-2. *Nanomaterials* **2021**, *638* (11), 1–19. https://doi.org/10.3390/nano11030638.

(69) Prasanna, V.L.; Vijayaraghavan, R. Insight into the Mechanism of Antibacterial Activity of ZnO: Surface Defects Mediated Reactive Oxygen Species Even in the Dark. *Langmuir* **2015**, *31* (33), 9155–9162. https://doi.org/10.1021/acs.langmuir.5b02266.

(70) Zhang, W.; Li, Y.; Niu, J.; Chen, Y. Photogeneration of Reactive Oxygen Species on Uncoated Silver, Gold, Nickel, and Silicon Nanoparticles and Their Antibacterial Effects. *Langmuir* **2013**, *29* (15), 4647–4651. https://doi.org/10.1021/la400500t.

(71) Li, Y.; Zhang, W.; Niu, J.; Chen, Y. Mechanism of Photogenerated Reactive Oxygen Species and Correlation with the Antibacterial Properties of Engineered Metal-Oxide Nanoparticles. *ACS Nano* **2012**, *6* (6), 5164–5173. https://doi.org/10.1021/nn300934k.

(72) Fujii, M.; Usui, M.; Hayashi, S.; Gross, E.; Kovalev, D.; Künzner, N.; Diener, J.; Timoshenko, V. Y. Chemical Reaction Mediated by Excited States of Si Nanocrystals—Singlet Oxygen Formation in Solution. *J. Appl. Phys.* **2004**, *95* (7), 3689–3693. https://doi.org/10.1063/1.1664021.

(73) Du, J.; Gebicki, J. M. Proteins Are Major Initial Cell Targets of Hydroxyl Free Radicals. *Int. J. Biochem. Cell Biol.* **2004**, *36* (11), 2334–2343. https://doi.org/10.1016/j.biocel.2004.05.012.

(74) Tian, Z.; Li, X.; Ma, Y.; Chen, T.; Xu, D.; Wang, B.; Qu, Y.; Gao, Y. Quantitatively Intrinsic Biomimetic Catalytic Activity of Nanocerias as Radical Scavengers and Their Ability against H_2O_2 and Doxorubicin-Induced Oxidative Stress. *ACS Appl. Mater. Interfaces* **2017**, *9* (28), 23342–23352. https://doi.org/10.1021/acsami.7b04761.

(75) Guo, R.; Fan, Y.; Tang, Y. Interesting Ag_3PO_4 Concave Rhombic Dodecahedra: The Same Face with Different Morphologies and Photocatalytic Properties. *RSC Adv.* **2017**, *7*, 23977–23981. https://doi.org/10.1039/c7ra02026k.

(76) Wang, H.; He, L.; Wang, L.; Hu, P.; Guo, L.; Han, X.; Li, J. Facile Synthesis of Ag_3PO_4 Tetrapod Microcrystals with an Increased Percentage of Exposed {110} Facets and Highly Efficient Photocatalytic Properties. *CrystEngComm* **2012**, *14*, 8342–8344. https://doi.org/10.1039/C2CE26366A.

(77) Wang, J.; Teng, F.; Chen, M.; Xu, J.; Song, Y.; Zhou, X. Facile Synthesis of Novel Ag_3PO_4 Tetrapods and the {110} Facets-Dominated Photocatalytic Activity. *CrystEngComm* **2013**, *15*, 39–42. https://doi.org/10.1039/C2CE26060C.

(78) Li, M.; Chen, M.; Wang, J.; Teng, F. Branching Growth of Novel Silver Phosphate Dendrites and the Greatly Improved Photocatalytic Activity by the Active {110} Facets. *CrystEngComm* **2014**, *16*, 1237–1240. https://doi.org/10.1039/C3CE41889H.

(79) Batvandi, M.; Haghighatzadeh, A.; Mazinani, B. Synthesis of Ag_3PO_4 Microstructures with Morphology-Dependent Optical and Photocatalytic Behaviors. *Appl. Phys. A* **2020**, *126*, 571. https://doi.org/10.1007/s00339-020-03761-6.

(80) Lipsky, F.; Lacerda, L. H. D. S.; De Lazaro, S. R.; Longo, E.; Andrés, J.; San-Miguel, M. A. Unraveling the Relationship between Exposed Surfaces and the Photocatalytic Activity of Ag_3PO_4: An in-Depth Theoretical Investigation. *RSC Adv.* **2020**, *10*, 30640–30649. https://doi.org/10.1039/d0ra06045c.

(81) Bi, Y.; Ouyang, S.; Umezawa, N.; Cao, J.; Ye, J. Facet Effect of Single-Crystalline Ag_3PO_4 Sub-Microcrystals on Photocatalytic Properties. *J. Am. Chem. Soc.* **2011**, *133* (17), 6490–6492. https://doi.org/10.1021/ja2002132.

(82) Bomio, M. R. D.; Tranquilin, R. L.; Motta, F. V; Paskocimas, C. A.; Nascimento, R. M.; Gracia, L.; Andres, J.; Longo, E. Toward Understanding the Photocatalytic Activity of $PbMoO_4$ Powders with Predominant (111), (100), (011), and (110) Facets. A Combined Experimental and Theoretical Study. *J. Phys. Chem. C* **2013**, *117* (41), 21382–21395. https://doi.org/10.1021/jp407416h.

(83) Lazzeri, M.; Vittadini, A.; Selloni, A. Structure and Energetics of Stoichiometric TiO_2 Anatase Surfaces. *Phys. Rev. B* **2001**, *63* (15), 155409. https://doi.org/10.1103/PhysRevB.63.155409.

(84) Eugen Schwarz, W. H. Richard F. Bader: Atoms in Molecules (A Quantum Theory) Clarendon Press 1990, Oxford. ISBN 019-855-1681, 438 Pages, Preis: 50. *Berichte der Bunsengesellschaft für Phys. Chemie* **1991**, *95* (10), 1308. https://doi.org/10.1002/bbpc.19910951039.

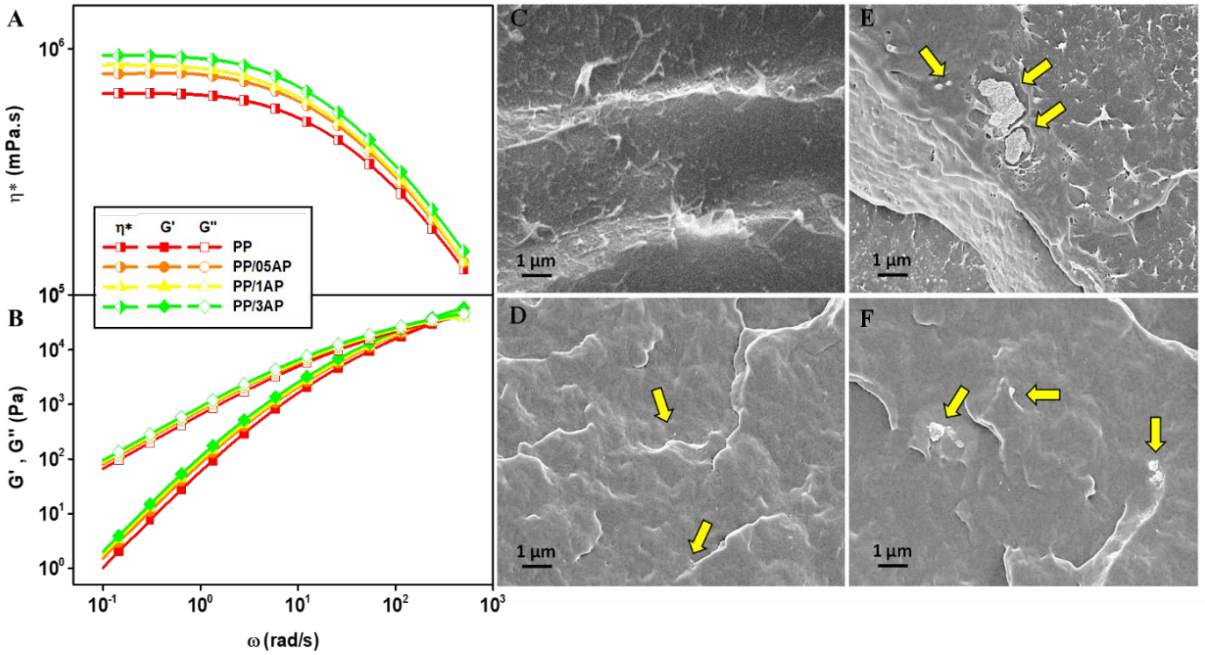

FIGURES AND TABLES

Figure SI-1 - (A) Complex viscosity as a function of frequency; (B) storage modulus (G') and loss modulus (G") of the samples; and cross-section SEM images of (C) PP, (D) PP/05AP, (E) PP/1AP and (F) PP/3AP.

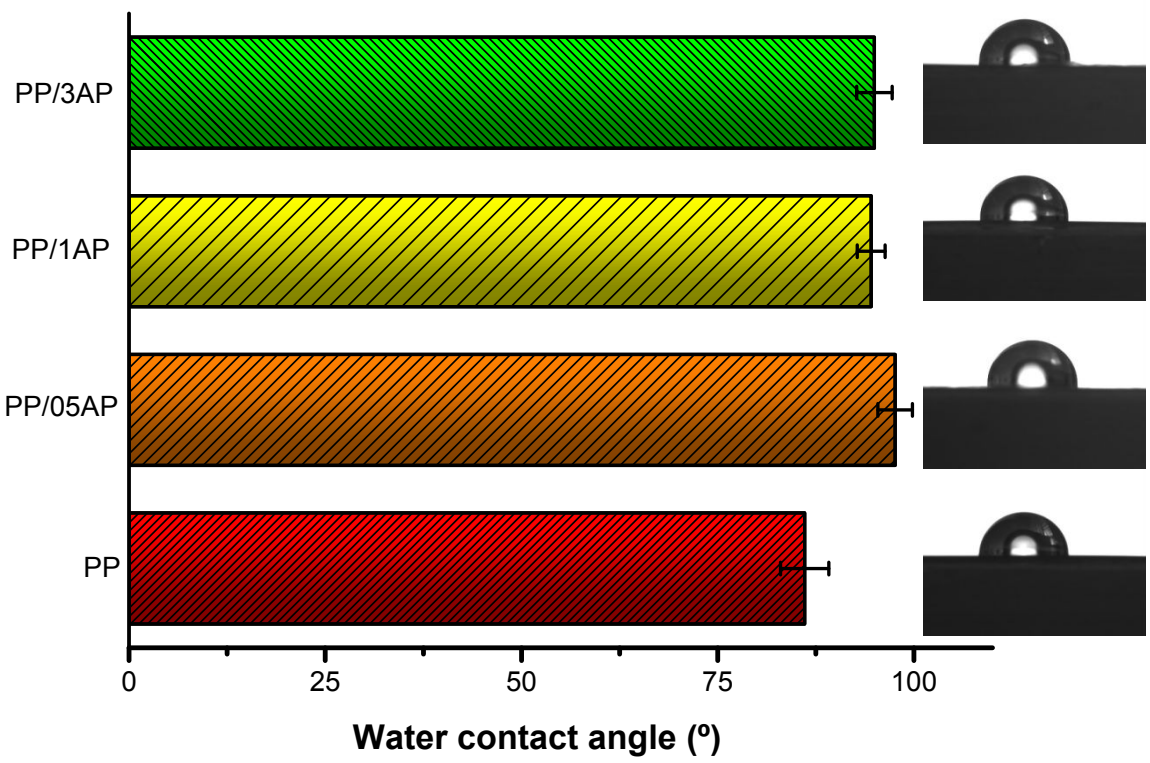

Figure 2 - Contact angle results of pristine PP, PP/05AP, PP/1AP and PP/3AP.

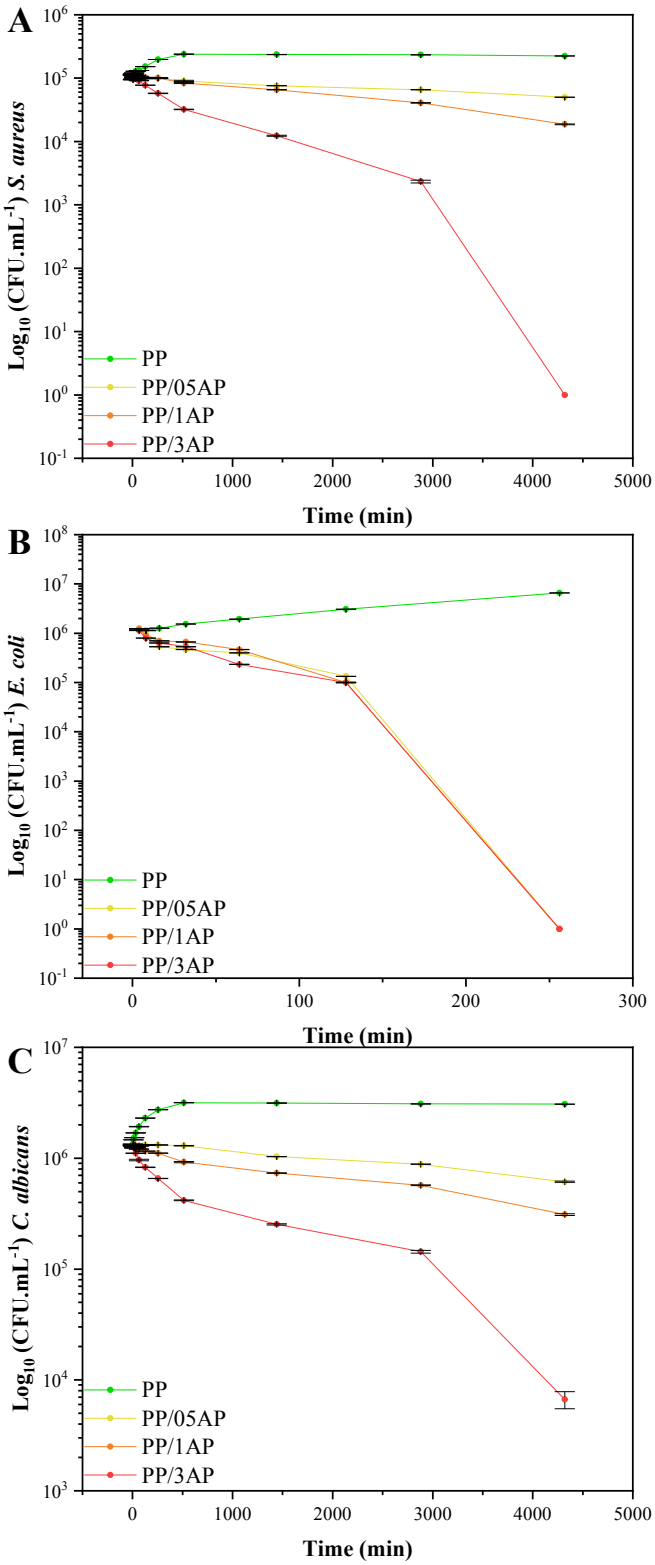

Figure 3 - Time–kill curves for (A) *S. aureus*, (B) *E. coli,* and (C) *C. albicans* using PP, PP/05AP, PP/1AP and PP/3AP samples.

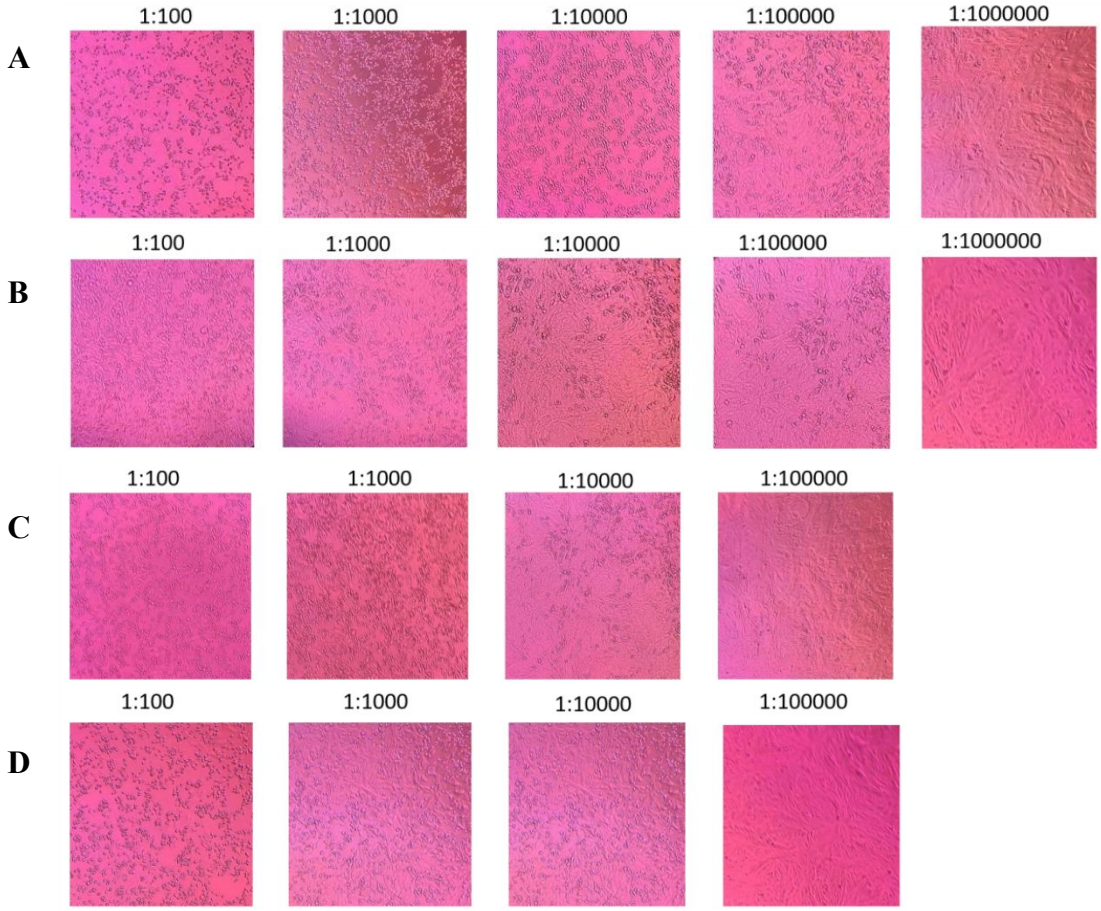

Figure 4 - Microscopic images of cell cultures incubated with viral dilutions in contact with (A) PP, (B) PP/05AP, (C) PP/1AP and (D) PP/3AP samples.

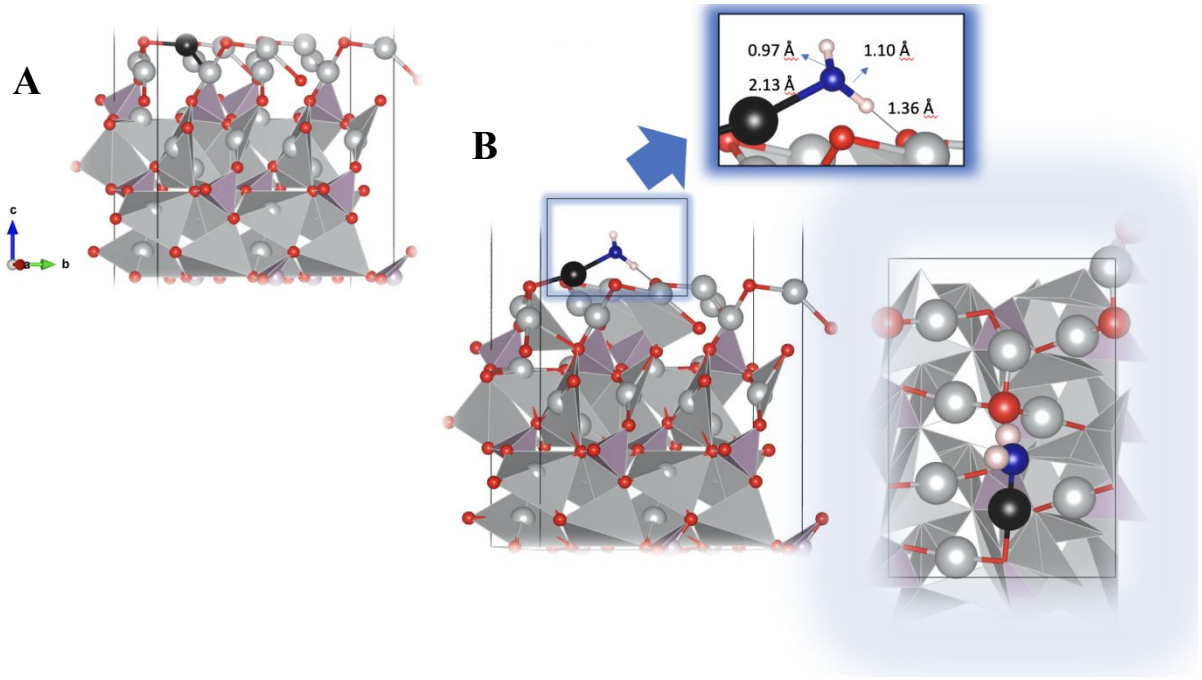

Figure 5 - (A) Side views of the relaxed clean Ag_3PO_4 (110) surface. The Ag cation where H_2O and O_2 adsorb is highlighted in black color; (B) side and top views of the H_2O adsorption system. O, P and Ag atoms on the surface are represented by red, violet and grey balls, respectively. For clarity, the O and H atoms of the H_2O are indicated in blue and white colors, respectively.

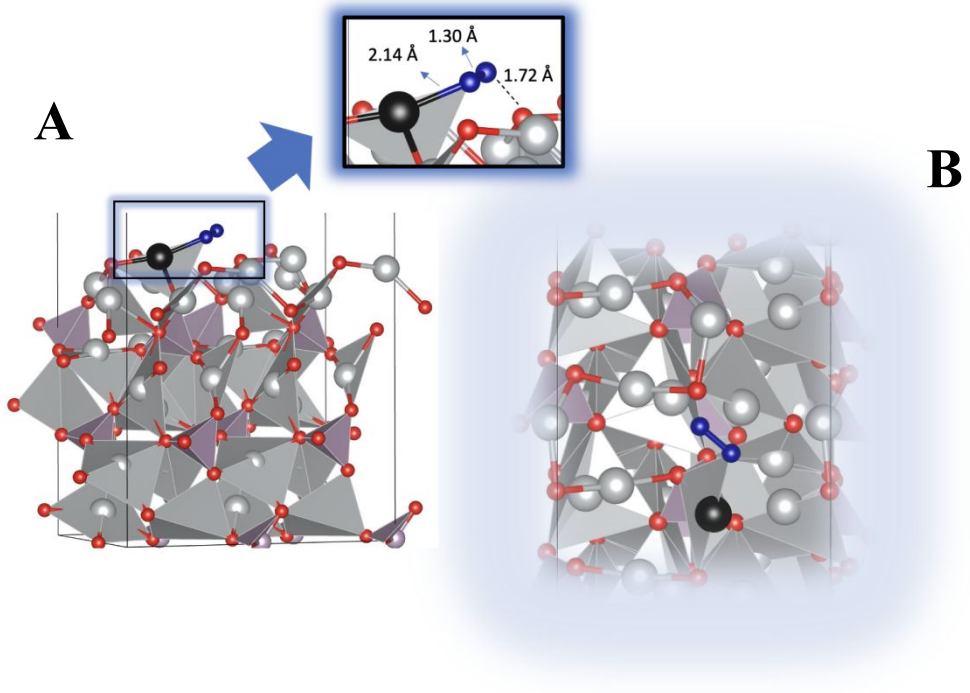

Figure 6 - Side (A) and top (B) views of one O_2 molecule adsorbed on the Ag_3PO_4 (110) surface. O, P and Ag atoms on the surface are represented by red, violet and grey balls, respectively. For clarity, the Ag adsorption site and the water O are colored in black and blue, respectively.

TOC Graphics